8 X-ray Spectroscopy, Photoelectron Spectroscopy, Auger Spectroscopy

X-ray spectroscopy, photoelectron spectroscopy and Auger spectroscopy measure the binding energies of the core-electrons, preferentially with wavelengths from 10^{-8} to 10^{-9} m, see Fig. 1.3, Chapter 1.The energy range of UV photoelectron spectroscopy lies in the same energy range as the binding or the ionisation-energy of the electron in the ^{1}H atom, and therefore belongs to the ultraviolet wavelength range of the optical spectrum. In comparison, the K-shell binding energies of much heavier atoms are up to four orders of magnitude higher than that for the hydrogen atom. The fermium-isotope ^{100}Fm has a K-shell binding energy of 143 keV. The main objective of the photoelectron spectroscopy (PES) is the measurement of extremely small changes in the binding energies of the inner electrons from 100 eV to 1000 eV, in order to study the chemical bonds between atoms, which have very weak influence on the binding energies of the core electrons.

The UV photoelectron spectroscopy works with the ultraviolet rays in the energy range between 5 and 40 eV (λ about 100 nm); whereas the X-ray photoelectron spectroscopy uses the energy range from 100 eV to up to 1500 eV. The X-ray spectral range is sub-divided into

- ultra-soft X-rays (λ > 1 nm, E < 1 keV),
- soft X-rays (1 – 0.1 nm, 1 keV < E < 10 keV),
- hard X-rays (0.1 – 0.01 nm, 10 keV < E < 100 keV),
- ultra-hard X-rays (λ < 0.01 nm, E > 100 keV).

X-ray tubes are mostly used for producing X-rays having energies in the range from soft to hard X-rays, while with the use of electron synchrotrons facilities the X-rays having energies varying continuously between the infrared radiation and extremely ultra-hard X-rays (10^{-5} > λ > bis 10^{-16}. The wavelengths of hard (for values of E > 14.4 keV) and ultra-hard X-rays overlaps significantly with the wavelengths of the nuclear γ-radiation, see Fig. 1.3.

Secondary X-rays are less absorbed (than secondary electrons) by condensed matter. Photoelectron spectroscopy (see Chapter 8.3) investigates surfaces, since the photoelectrons penetrate only 10^{-9} m, whereas the so-called X-ray spectroscopic methods (see Chapter 8.2) investigate samples with a thickness 10^{-6}–10^{-2} m. All these spectroscopic methods are essentially applied to solids or to molecules adsorbed on solids. In the University of Leipzig, these techniques were established by Professor Meisel and Professor Szargan in the Institute for Physical Chemistry II.

8.1 X-ray tubes and synchrotron radiation

In an X-ray tube a high voltage U accelerates the electrons emitting from the cathode. The anode material slows down (deutsch: *bremsen*) the electrons. This creates the so-called *Bremsstrahlung*, continuous X-rays with an upper limit on the frequency ν or lower limit of the wave length λ given by the relation $hc_0 / \lambda = h\nu = eU$, where e is the elementary electron charge, h the Planck's constant, and c_0 the vacuum velocity of light . For U = 50 kV we have $\lambda = 2{,}5 \times 10^{-11}$ m. Superimposed to the *Bremsstrahlung* is an element-characteristic-emission spectrum. The limited electrons radiate energy according to the laws of classical electrodynamics like a "Hertzian Dipole", i.e. predominantly perpendicular to the direction of retardation or original acceleration. Therefore, the anode surface is positioned at an inclination angle of 45° to this direction.

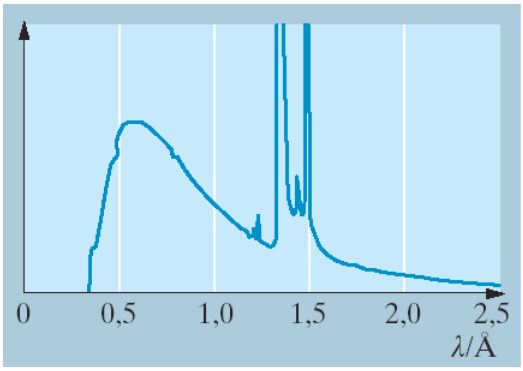

Fig. 8.1 X-ray spectrum of Cu-anode shown together with the continuous 'Bremstrahlung' superimposed with the characteristic K_α und K_β lines of the copper anode. Tube-voltage 38 kV. Taken from Meschede: Gerthsen Physik, 22nd Edition, Fig.15.21.

Figure 8.2 below demonstrates the analogy between the characteristic X-ray spectrum and the alkali spectrum. This analogy is based upon the fact that in a single particle picture the positron equally describes the missing electron in an otherwise completely filled shell. The value or the name of the lower quantum level to which the observed transition occurs is used to characterize and label the lines (and edges) observed in the X-ray spectrum, e.g. for the transitions to lower quantum levels n = 1, 2, 3, 4, 5 the series is named as K-, L-, M-, N-, O-series, respectively. Any further transitions to next higher levels, corresponding to an increase in angular momentum by unity, are indexed viz. designated as α, α' and so on, or otherwise as α1, α2. Levels with n > 1 split up apart due to the difference in angular quantum number or spin quantum numbers.

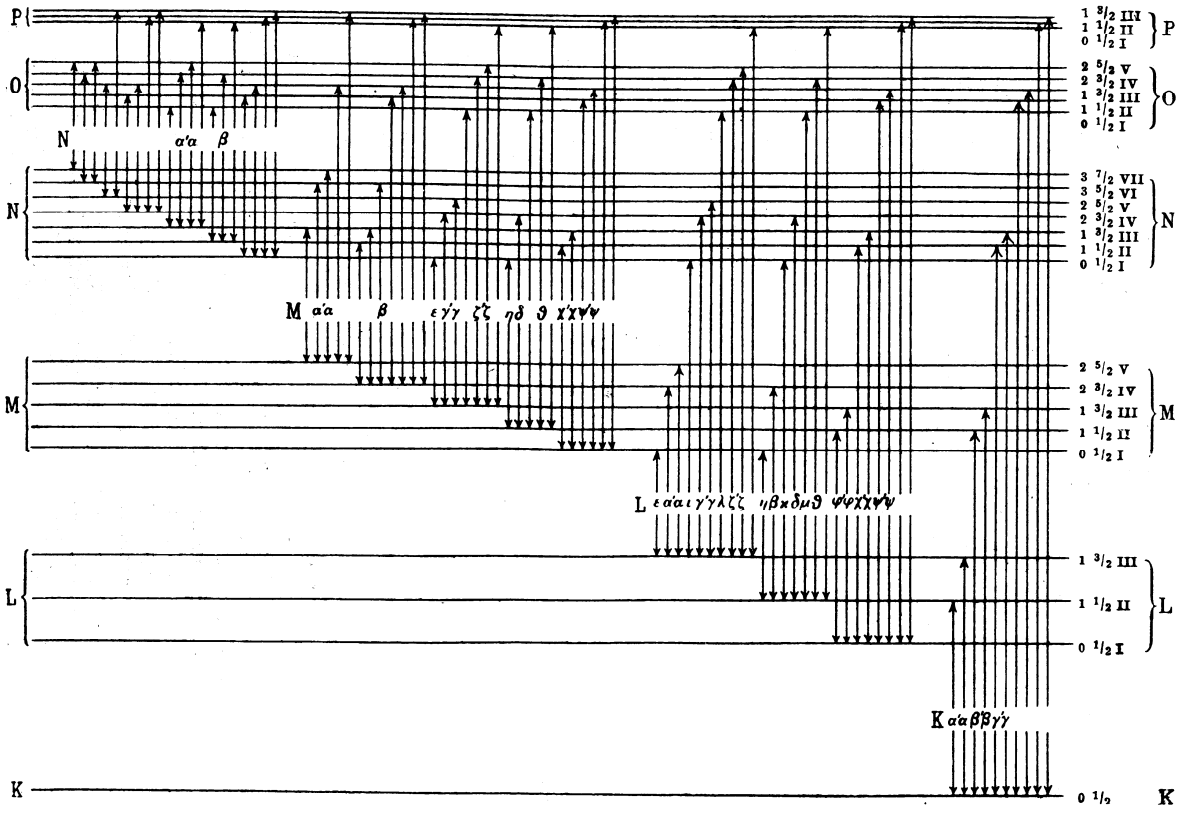

Fig. 8.2 Detailed illustration of X-ray- term schemes showing spectral-transitions and quantum numbers. The first number on right represents the quantum number ℓ, and the second one the quantum number j. The character K stands for n = 1, n = 2 and so on. Taken from W. Finkelnburg, Einführung in die Atomphysik, 4. Aufl. Abb. 67.

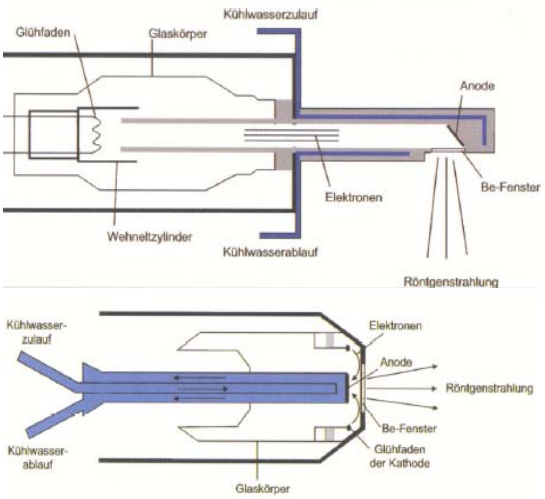

Fig. 8.3 Side-window tube and end-window tube for X-ray fluorescence analysis (XFA). Taken from a publication by Janßen und Flock, see literature. In the illustration on top the anode is kept at a ground potential which allows for a simpler cooling mechanism using ordinary water. In the same way, in the end-window tube the cathode is kept at ground potential.

In the X-ray fluorescence analysis (XFA) the use of usual X-ray tubes is made as sketched in Fig. 8.3 with applied voltages ranging between 50 to 100 kV. Thereby, we make use of the continuous X-ray radiation, viz. "Bremsspektrum", as well as the discrete spectrum, as far as it has energies above the transition energies of the material under study.

The discrete spectrum of ordinary X-ray tubes can be used as radiation source for the photoelectron spectroscopy, which will be discussed in Chapter 8.3. Most frequently the Al-$K_{\alpha 1,2}$-lines with energies between 1486.70 eV and 1486.27 eV and an energy spectrum width about 0,85 eV are used for this purpose. A crystal monochromator, cf. Fig. 8.4, is used to reduce the spectral width to a full width half maximum value of around 0.25 eV.

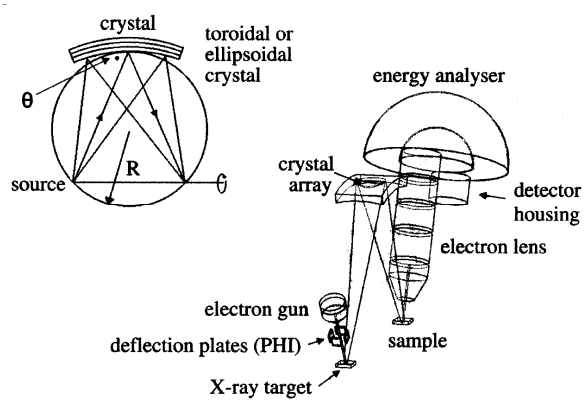

Fig. 8.4 X-ray monochromator for photoelectron spectroscopy. Taken from I.W. Drummond, see Literature.
Left: The Bragg's geometry of a curved crystal that for a given frequency can be used to focus the radiation from anode onto the position of the probe.
Right: Integration of the monochromator in the spectrometer arrangement, see Chapter 8.3.

More monochromatic X-rays with high power and continuously-varying energies can be obtained from synchrotron radiation. Electrons circulating in storage rings are accelerated to a velocity near to the light velocity; and the radial-acceleration by the deflecting magnets causes the so-called "magnetic Bremsstrahlung" of the relativistic-electrons. This radiation has very a high energy density, very little beam-divergence (reciprocal of electron energies, for e.g. 0.5 mrad for 1GeV), is strongly polarized, and covers a wide energy range from the optical spectrum to 10 keV (also above 100 keV, when the electron energies in the circulation rings can be raised above 5 GeV). Thereafter, series of multiple reflections at crystal lattices are used to obtain the desired pure-monochromatic radiation. The pulsed synchrotron radiation, continuously generated by the electron-packets going around in circular paths, is then radiated into corners of specially constructed storage rings in very narrow packets (10^{-4} rad), see Fig. 8.5.

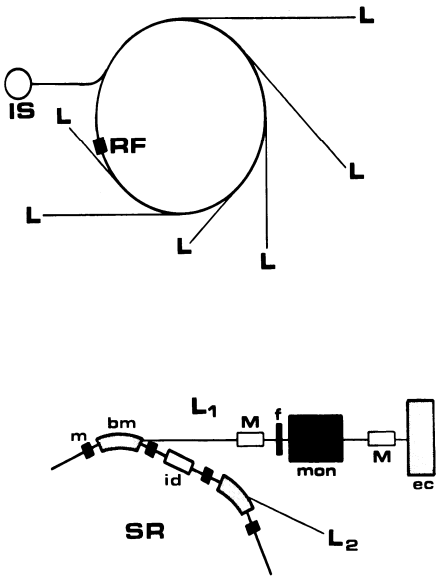

Fig. 8.5. Schematic diagram of a synchrotron-radiation source taken from Giorgio Margaritondo, see Literature. The top-figure shows the injection system (**IS**), which is separate from the main storage ring. It is used to inject electrons into the main storage ring, if its electron current has been decreased after some hours. The in-built radio frequency cells (**RF**) serve to compensate the velocity-losses due to radial acceleration of electrons after each single-round through storage ring. Such cells are also used to accelerate the electrons in the injection system. In the main storage ring (**SR**) we see 6 main work-lines, viz. beam-lines designated as L, and one from them is named (**L_1**). The electrons are kept in the straight trajectory through the use of quadrupole-magnets (**m**), whereas dipole-deflection-magnets (bm, benching magnets) are used to deflect (radially-accelerate) cor4responding to the curvature of circular storage ring. The beam line L_1 contains special focussing and de-focussing mirrors (**M**, mirror), filter (**f**) and Monochromator (**mon**).

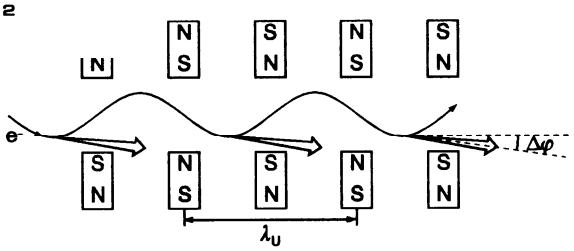

Abb. 8.6. Wiggler-arrangement, taken from Kuzmany, see Literature.

Every beam line ends in one, usually uncomfortable and small, experimental chamber (**ec**), that is normally fully occupied by the experiment- related-equipments with almost little free space for anything else.

Figure 8.5 shows an inversion device (id) in the beam line L2. This device drastically improves the intensity and monochromaticity of the incoming radiation and increases the resolution of the experiment to a value better than 50 meV. The *n* alternating magnetic fields of a "wiggling magnet", see Fig. 8.6, produce an *n*-times intense radiation. Its energy depends on the distance of separation amongst the consecutive magnets. If the number of magnets is very large (around 100), then highly coherent radiations, due to interference effects in certain specific directions for certain wavelengths, can be achieved. The peak intensity is proportional to n^2. The1 to 2 meter long series of alternatively arranged magnets is designated as "Undulator".

An explanation of the "magnetic Bremsstrahlung" demands a relativistic consideration of the electrodynamics involved. For usual X-rays the speed of the electrons is very small as compared to the velocity of light and the radiation of the x-rays is as that of an ordinary Hertzian dipole, that means perpendicular to the direction of acceleration in a relatively wide radiation angle.

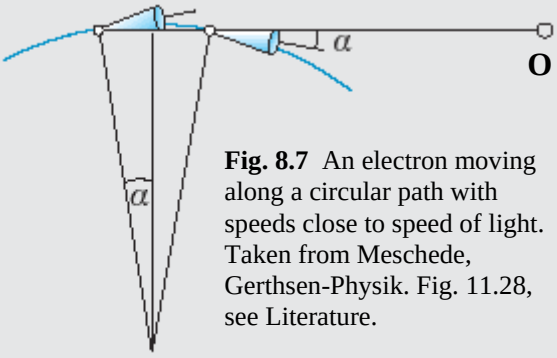

Fig. 8.7 An electron moving along a circular path with speeds close to speed of light. Taken from Meschede, Gerthsen-Physik. Fig. 11.28, see Literature.

Electrons circulating in storage rings are accelerated to a velocity near to the light velocity. The storage ring has a radius of curvature r. The radiation cone's opening angle is given by the relation $2\alpha \approx 2m_0c_0^2/E$. Since the accelerated electrons inside a synchrotron have energies many-times larger than the rest energy of a electron ($E_0 = m_0c_0^2$) the cone's opening angle is very small (0.5 mrad for 1 GeV), see Fig. 8.7. The circulation frequency given by ω_0 is given nearly as $\omega_0 = c_0/r$. An observer located at point **O** in Fig. 8.7 sees the clock-wise circulating electron as a flash of light passing by him, which starts when the beginning of the bundle is to the left of him and ends when its tail-part crosses to his right. The respective circular paths or arcs have a length given as $2\alpha r$ and would complete one-turn around the ring in a time given by relation $t_1 = 2r\alpha/c_0$. The pulse of light from the left side must, however, in comparison to the light from the right side additionally cover a distance of circles chord given by $2r \sin\alpha$, which requires the substitution $t_2 = 2r \sin\alpha/c_0$. This represents for the observer at that place a time period in which a flash of light goes across him

$$\Delta t = t_1 - t_2 = (2\alpha - 2\sin\alpha)\, r/c_0 \approx \frac{r\alpha^3}{3c_0}. \qquad (8.01)$$

An impulse lasting for time Δt has a full width half maximum (FWHM) at peak of frequency spectrum of $1/\Delta t$. That gives us a bandwidth of $\Delta\omega \approx 1/\Delta t \approx 3c_0/(r\alpha^3) \approx 3cE^3/(rE_0^3)$. We thereby find, by using the previously calculated values, that the bandwidth for electrons having energies in range of 5GeV is almost 10^{12} times higher as compared to the angular frequency of electrons as given by the relation $\omega_0 = c_0/r$, which thus delivers discrete frequency separations in th Megahertz range. That gives us a quasi-continuous spectrum of frequencies in the range $\omega_0 E^3/E_0^3$.

For calculating the efficiency we make use of an equation similat to equ. (2.55):

$$\langle P_{\text{em}} \rangle = \frac{\omega'^4\mu^2}{6\pi\varepsilon_0 c_0^3} = \frac{\omega'^4 e^2 r^2}{6\pi\varepsilon_0 c_0^3} = \frac{e^2 c_0}{6\pi\varepsilon_0 r^2\alpha^4} \approx \frac{e^2 c_0\, E^4}{6\pi\varepsilon_0 r^2 E_0^4}. \qquad (8.02)$$

Thereby, the dipole-moment μ is replaced with the product of the electric charge and radius of the electron's orbit. In case of angular frequency, a corrected value $\omega' = c_0/(r\alpha) = \omega_0/\alpha$ is used instead of ω_0, which takes into account that relativistic electron emits radiation in packets and short pulses only in small angular arcs of length $2\alpha r$ (impulse-action), and not along the entire circumference of the electrons orbit.

Referring back to the equ. (2.08) we can understand that the reduction of the radius of the electrons orbit leads to an increase in the power and intensity of the Synchrotron's radiation. Big and huge magnets of iron can however, attain a relatively small field of 1 T. Equating the Lorentz force to the centrifugal force we have $p/r = ev/r = eB$. The relativistic energy (ignoring the e's rest mass energy) $E = pc_0$ gives $r = E/(eBc_0)$ and for $B = 1$ T and $E = 100$ GeV a radius of around 300 m. The use of superconducting Wiggler magnets enables a reduction in the radius by one order of magnitude, which gives an increased effective power output that is two orders of magnitude higher, see equ. (8.02).

8.2 X-ray spectroscopic methods

X-ray emission spectroscopy (XES) deals with the traditional X-ray emission analysis and the modern X-ray fluorescence analysis. In the former method the sample to be analyzed is bombarded with the electrons in an X-ray tube. Thereby, the probe, which is positioned at the anode of the tube, suffers damage, or sometimes even destroyed. However, fluorescence X-ray analysis techniques has effectively replaced the earlier method of emission-spectra analysis of the probe positioned at the position of anode because of the problems and technical-difficulties involved in sample preparation, as also due to shorter destruction lifetimes.

X-ray fluorescence analysis (XRF) uses a cold excitation of electrons in the probe by the application of the *Bremsspektrum* mostly of a rhodium anode. Thus, as the sample is not directly bombarded with incoming high energy beam of electrons, but with low energy beam therefore in this technique the probe suffers less damage then in the previous techniques. The fluorescence output, or intensity, increases by a factor between 10% for the case of light-elements with atomic number $Z = 20$ to up to 90% for heavier elements with $Z = 80$ (K-series). As is the normal practice the crystal spectrometer is installed either with the proportional counter or scintillation counter.

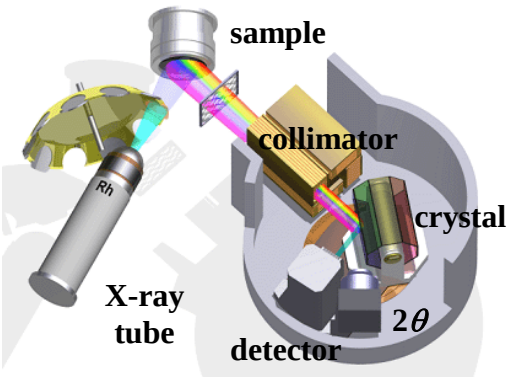

Fig. 8.8. Experimental set-up of a spectrometer for X-ray fluorescence investigations. This illustration has been taken from the BRUKER AXS.

The crystal surface is positioned at an inclination angle θ to the direction of the collimated parallel beam, and the intensity of the beam reflected from the crystal is then measured as a function of the angle θ.

For the distance d of separation between the crystal planes the wavelength dependence of the diffracted light is given by Bragg's condition

$$2d \sin\theta = m\lambda. \tag{8.03}$$

The order of diffraction is denoted by m. The first order $m = 1$ is used for the detection. Instead of the crystal detector an energy-dispersive semiconductor-detector can be used, in order to exploit a greater spatial-spread of the fluorescence radiation.
(AXS_History.ppt, Bruker_RFA.ppt, RFA_Janssen.pdf, The related data files can be sent to the interested students in the case of a special request from them.)

X-ray absorption spectra (XAS) are obtained by transitions of inner-orbital, or core-, electrons to vacant outer-orbitals under the influence of continuous irradiation by a *Bremsspektrum*. The lowest unoccupied energy levels are at very small distance of separation from the next higher levels and to the continuum of the free-electron energy levels, which have arbitrary kinetic energy. Therefore, we get broad absorption edges in place of the sharp and discrete line spectrum. The edges obey like the line spectrum the Moseley's law

$$\tilde{\nu} = \frac{1}{\lambda} = R(Z-\sigma)^2\left(\frac{1}{n''^2} - \frac{1}{n'^2}\right). \tag{8.04}$$

R stands for the Rydberg's constant and *Z* for the atomic number of the element. The screening constant σ means in the case of $\sigma = 1$ that apart from the ejected electron in the K_α –shell a further (deep-lying) exists which happens to screen the nuclear charge with an elementary charge. For the L_α-line the experimentally obtained value is $\sigma = 7.4$; the charge shielding effect in this case has 2 + 7electrons. With $\sigma = 1$ for K_α, we get the following special case of the Moseley's law:

$$\tilde{\nu} = \frac{3}{4} R\,(Z-1)^2 \quad \text{for the } K_\alpha\text{-emissions line and} \tag{8.05}$$

$$\tilde{\nu} = R\,(Z-1)^2 \quad \text{for the K-absorptions edge.} \tag{8.06}$$

However, the absorption method is not so suitable for characterizing a substance with a good resolution due to the broad edges that are produced by this technique. But the analytical analysis of the absorption edges, of so-called **XFAS** (X-ray absorption fine structure), has established itself as a precise investigation technique in the field of non-crystalline materials for probing inner spatial- structure and dynamics of and in-vicinity of the observed atoms. The field of **XFAS** is further classified for investigations directly above the threshold energy (i.e. upto 30 eV) of the absorption edges, into the sub-domains of **XANES** (X-ray absorption near edge structure) or **NEXAFS** (near edge X-ray absorption fine structure), while for investigations about 40–1000eV above the threshold energy is designated as **EXFAS** (extended X-ray absorption fine structure).

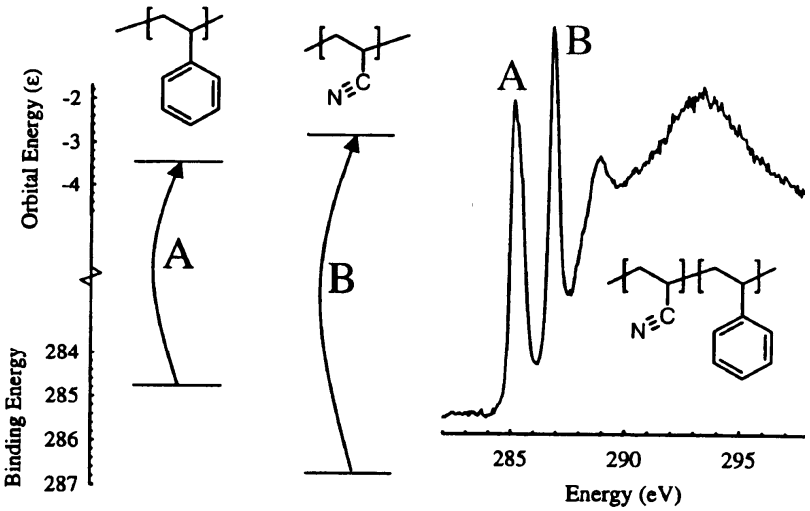

Fig. 8.9 NEXAFS image of Poly-(Styren-r-Acrylonitril), taken from a publication from Harald Ade und Stephen Urquhart, cf. literature index at the end of this chapter. The figure shows NEXAFS of poly-(styren-*r*-acrylonitril) and contains two sharp lines A (phenyl group) and B (acrylonitril group) for the transition from C-1s-orbitalen to the π*-LUMO-orbital (lowest unfilled molecular orbital) as also on high-energy side a poor un-resolved signal for the transition to the σ*-orbitals.

The techniques of NEXFAS and XANES give general information about the lowest unoccupied orbitals, about the electronic configuration, and the coordination number of the absorbing atom. Although the techniques of NEXAFS und XANES in principal are very much similar, the first technique is strongly established for investigations done with soft x-rays of the carbon atoms in polymers or even for molecules absorbed on the top surface of solid state, while the second technique of XANES is applied mostly for relatively bigger atoms which absorb hard x-rays, i.e. for investigations with hard x-rays.

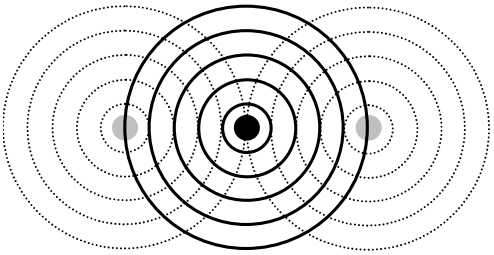

Fig. 8.10 A one-dimensional model of the XAFS-process. The Photoelectron from the excited central atom is scattered by the neighboring atoms and thereby it produces an interference pattern between the frontward and backward propagating waves, which thereby modulate the energy of the generated photoelectron in dependence of its distance from the atoms.

The X-ray absorption fine structure about 40 eV above the threshold edge (EXAFS), occurs due to the energy difference between the electrons near to the nucleus and the final state of the emitted photoelectrons, *which can be easily regarded as spherical waves emitted by the atom involved*. These waves, whose frequency obviously depends on the frequency of the absorbed light, are backscattered by all of the neighboring atoms (also termed as **MS**, which stands for *multiple scattering*). This interference of the outgoing and the neighboring atoms-scattered waves, *or even partially reflected waves*, leads to modulation of the energy of the photoelectron in dependence on the energy of the radiated x-rays.

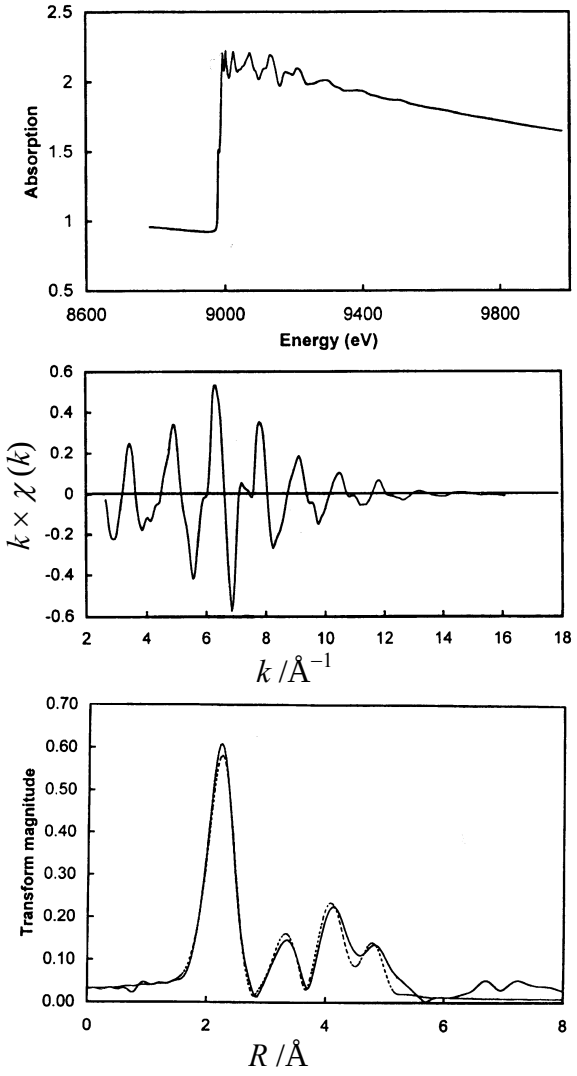

Fig. 8.11: XAFS of Cu-K-edge, taken from a publication from Steve M. Heald and D.T Jiang, Pls. See literature. The fig. on top shows the measured absorption-spectrum, spectrum in the middle the normalized absorption $\chi(k)$, which has been multiplied with *k in order to impart more importance to higher k*-values, as a function of the wave-number k of the photoelectron, Pls. see text below. The fig. at the bottom depicts the four peaks obtained after Fourier-transformation all of which correspond to the distance of separation amongst the first four shells in a copper atom (The fit to the measurement is indicated with a broken-line).

Figure 8.11 demonstrates how **EXFAS** determinates atomic distances inn amorphous materials. The usual technique for structure dtermination is X-ray diffraction (**XRD**) which can be hardly applied to amorphous materials. The variable in the picture on the top in fig. 8.11 is the energy of the absorbed X-rays. In the middle picture the wave-number of the generated photoelectron is the variable. The wave-number $k = 2\pi / \lambda$ includes the de Broglie-wavelength $\lambda = h/p = h/(m_e v)$, where m_e is the mass of the excited atom or molecule which emits the photoelectron.

The velocity v can be easily determined from the kinetic energy $E_{\text{kin}} = m_e v^2$. We obtain for the wave number of the photoelectron

$$k = \frac{\sqrt{2m_e E_{\text{kin}}}}{\hbar}. \tag{8.07}$$

The kinetic energy E_{kin} can be determined from the difference between the measured energy of the irradiated X-rays and the electrons binding energy. However, the binding energy of the electron is not so accurately known, and hence there exists a problem in definition of the k-scale, which is mostly given in the units of Å^{-1}.

Conventionally, the factor for X-ray absorption is denoted as $\mu(\lambda)$, and $\mu_0(\lambda)$ stands for the hypothetical absorption by an atom assumed to be fully isolated and completely free of any interaction with neighboring atoms. This last term would lead to the top-illustration in Fig. 8.11 smoothening of the oscillations above the absorptions-edge. Thereby, we define the normalized X-ray absorption by the relation

$$\chi(k) = \frac{\mu(k) - \mu_0(k)}{\mu_0(k)}, \tag{8.08}$$

which takes into account the correction needed for the exclusion of the background signal. A multiplication of the function $\chi(k)$ with k in first, second or third order (in first-order in the middle picture of Fig. 8.11 and in second order for Fourier transformation used to obtain the illustration at bottom) creates a filter, which leads to a narrowing (better resolution) of the signal after the Fourier transformation. Equation (8.09) should illustrate through the presence of the sine term, why the Fourier transformation of absorption factor, $\chi(k)$, gives us a relation which is a function of distance R_i of any given scattering center from the atomic-nucleus under consideration.

$$\chi(k) = \sum_i \frac{N_i}{kR_i^2} F_i(k)\, exp\left(-\Delta k^2 \frac{k_B T}{m_r \omega^2}\right) exp(-2R_i/\lambda)\ \ sin\left[2kR_i + \psi_i(k)\right]. \tag{8.09}$$

Equation (8.09) was given in a similar form by E.A. Stern, Phys. Rev. B10 (1974) 3027. The present form is adopted from a work by Heald and Jiang on pages 770/771, see list of references. The above equation is valid for the case of excitation of a single-photoelectron by an non-polarized light (as also for linearly polarized light with triple- or multiple- axis symmetry of the central atom) and a small quantum of disorder amongst the neighboring atoms, whereby the emitted photoelectron happens to suffer only a single collision or scattering event before it is backscattered to the initial central atom (i.e. ignoring multiple scattering). Here, R_i is the distance of separation between the i^{th} scattering atom and the central atom under consideration. N_i is the number of the scattering atom at a distance of R_i. The factor $F_i(k) \exp(-\Delta k^2 k_B T/m_r \omega^2)$ represents the amplitude of the backscattered from the neighboring atom i with a corresponding Debye-Waller-factor $\exp(-\Delta k^2 k_B T/m_r \omega^2)$. The last term assumes the probability of the final state of the lattice vibrations being identical and exactly the same as the initial state before the scattering process, i. e. it considers the case of an elastic collision. This factor remains valid for the case of harmonic lattice vibrations having angular frequency ω, reduced mass m_r, and temperature T – which has values sufficiently high above the absolute zero. The term Δk denotes the change of the wave vector due to the scattering process. The term $\exp(-2R_i/\lambda)$ takes into account the inelastic losses due to the scattering process caused by the neighboring atoms and in the space between them, where λ represents an averaged mean value of wavelength for the case of a free electron. The dependence on the distance of separation amongst the atoms is given explicitly by the term $1/kR_i^2$. The sinusoidal modulation factor, which is important for the Fourier

transformation consists of the term $2kR_i$ and the phase shift $\psi_i(k)$, which include contributions from the central atom and from the i^{th} backscattering atom.

The distribution of the spatial periodicity of the scattering centers, obtained as a result of Fourier transformation in the *k*-space, includes a shift in the real space due to the phase shift $\psi_i(k)$. It was, earlier used to be corrected with the help of a calibration-substance. However, modern computational power and simulation techniques allow us to avoid this arbitrariness associated with the calibration done with a different substance, as also to take into account the event of multiple scattering. The scattering factor f_{eff} (program name FEFF), which has a directional dependence in place of *F* in the Eq. (8.07) takes into due consideration the important terms of phase shift, see Rehr et al. in the Literature.

8.3 Photoelectron spectroscopy (PES)

The PES technique is used to measure the kinetic energies of the electrons, which have been completely ejected out by photons either from inner core-orbitals or from outer valence shells by X-rays or UV radiation, respectively. It is known that inner electrons of larger atoms are not directly involved in the formation of chemical bonds. Nevertheless, their energy is sensitive to the effects of chemical bonds under the influence of the potential exerted on them by the external or valence electrons. Therefore the photoelectron spectroscopy (**PES)** has been termed "Electron Spectroscopy for Chemical Analysis (**ESCA**)" by its original founder Kai Manne Börje Siegbahn. The main emphasis of its applications lies in diverse fields, beginning from the techniques used for the determination of binding states of free molecules to the analysis of the shifts in the electron energies in the solid state of matter. This is the reason why the designations PES, UPS and XPS dominate in the literature now.

By employing UV radiation (mercury, or xenon gas discharge lamps, or also with synchrotron radiation) in the ultraviolet photoelectron spectroscopy (UPS), we can attain very high resolution better than the usual limit of 30 meV, in special cases even as narrow as 3 meV. This lies between the frequency-spectrum range of far-infrared and microwaves. It means that for example even rotational-vibrational motions can be analyzed by UPS, if they cannot be excited either in the infrared (IR) or Raman spectroscopy.

For the X-rays excited photoelectrons (XPS, X-ray photoelectron spectroscopy), the resolution is usually not better than 500 meV, and with crystal-monochromator a little better and down to about 250 meV. With some efforts it is possible to improve the resolution drastically to some tens of meV by synchrotron radiation and implementation of special monochromator techniques. Because of the smaller penetration depths of the photoelectrons (about 1 nm), the techniques of PES are predominantly employed for analysis and studies of surfaces in the solid state.

The number of electrons that have been created due to the photoelectric effect as a function of their kinetic energy, or velocity, is measured in photoelectron spectroscopy (as also in the case of Auger spectroscopy, cf. Chapter 8.4).

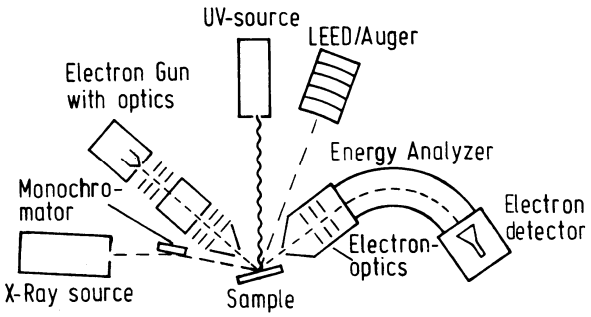

Fig. 8.12 Schematics of arrangement of equipment for investigation with slow electrons. Taken from S. Hüfner, see Literature.

In Fig. 8.12, the X-ray and UV radiators belong to the PES, whereas the electron-gun and LEED/Auger are used for the EELS

(electron energy loss spectroscopy) in LEED (low energy electron diffraction). EELS and LEED are not included in this lecture. For the Auger Spectroscopy see Chapter 8.4. The electron-optics, the energy-analyser and electron-detector are utilized for all of the above mentioned techniques. Therefore we find all of these above mentioned instruments together in a single experimental set-up. A capacitor made from two hollow concentric hemi-spherical shaped balls of different radius is employed as an energy analyzer, which enables us to obtain information about incoming electrons energies by the methods of variable (through the control of potential across capacitor) directional-focussing of electrons.

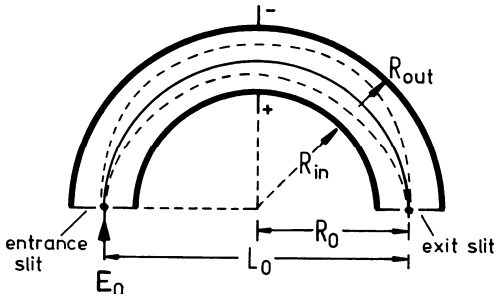

Fig. 8.13 Spherical deflection-analyzer, taken from A. Barrie, see Literature

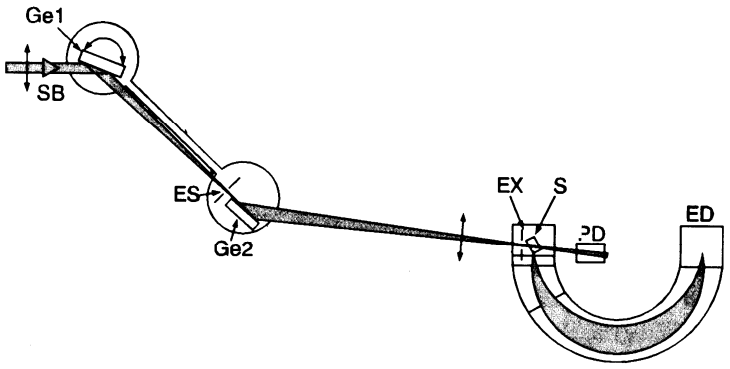

Fig. 8.14 XPS with Synchrotron radiation. SB denotes the entry point of *synchrotron beam*. Ge1 und Ge2 denotes the Germanium-two-crystal-diffractometer monochromators, where the incoming diffraction ES is focused onto the outgoing diffracted beam EX. S denotes the sample, PD the photo detektor and ED the electron detector. Taken from Kuzmany, see Literature.

The sample is irradiated with monochromatic photons. The electron detector at the exit of the spectrometer registers a signal only for incoming photo-electrons with a certain velocity or E_{kin}, which can be adjusted by the voltage of the spherical deflection-analyzer. E_{kin} is equal to the difference of energy between the energy $h\nu$ of the incoming radiation and the binding energy $E_B(k)$ *of the* k-shell. If we define the binding energy as the difference of energies between the final state and the initial state, which refers to the case of transition from the state with $N-1$electrons to the state with N electrons, we obtain $E_B(k) = E_f^{N-1}(k) - E_i^N$ and this gives us further

$$E_{kin}(k) = h\nu - E_B(k) = h\nu - [E_f^{N-1}(k) - E_i^N]. \qquad (8.10)$$

In this notation of the binding energy the corresponding energy is calculated with reference to the vacuum level, which is an appropriate assumption for a free atom or a molecule. In solid state more often the energy is calculated from the Fermi-levels as a reference level. In this case, we have to subtract the term relating to the work function on the right hand side of equ. (8.10). Figure 8.15 shows the spectrum observed of the L-gap from precious metals, where the binding energy has been referred to the Fermi energy level.
E_B is always positive, while the orbital energy $\varepsilon(k)$ is defined to have a negative magnitude. Unfortunately, the two magnitudes are not identical. The binding energy is experimentally

obtained. But the orbital energy is slightly different. When a X-ray photon is absorbed, a photoelectron is created with a well defined kinetic energy and there remains a positively charged and almost immobile ion behind. However, the state of lattice vibrations in the crystal changes and this phenomenon has to be taken into account for in the highly resolved UPS spectra. As in the initial state we have $v'' = 0$, we have to add the term $E_{vibr}(v') - E_{vibr}(v'' = 0)$ on the right hand side of the equation (8.10). Fig. 8.16 shows the spectrum from a HCl molecule due to the vibrational and rotational motion of structure.

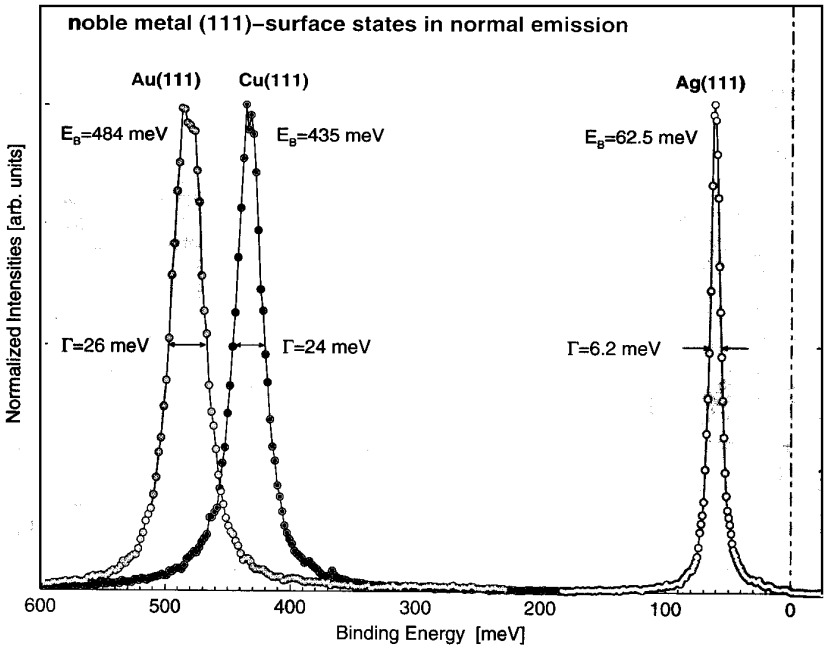

Fig. 8.15 L-gap.The surface states of an (111)-surface of a precious metal, taken from Fig. 1.28, S. Hüfner, see Literature.

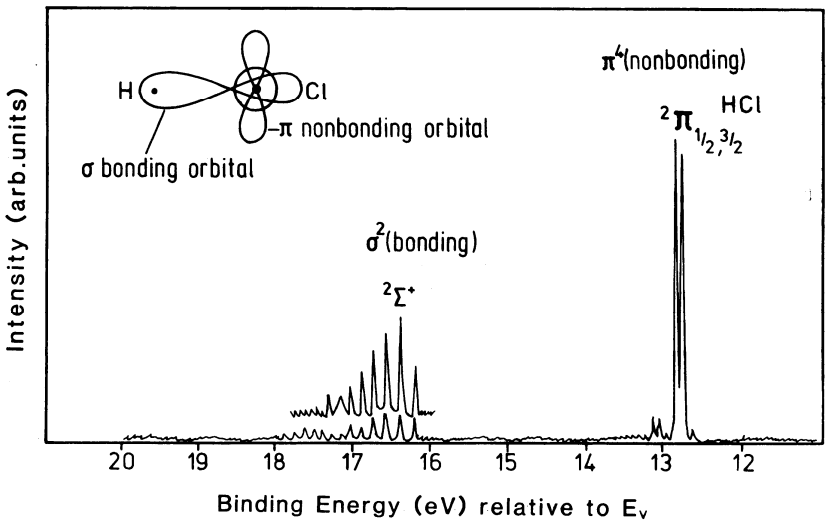

Fig. 8.16 HCl, a 21.2 eV-UPS-spectrum, taken from Fig. 5.8, S. Hüfner, see Literature.

The essential reason for the difference between $E_B(k)$ and $-\varepsilon(k)$ is however the relaxation effect that occurs inside the orbital planes of an atom after an electron has been removed from the atom.

The corrected value of E_i^N, is given by equ. (8.11), where relativistic effects are still ignored:

$$E_i^N = E_{i\,HF}^N + E_{i\,correlation}^N. \tag{8.11}$$

$E_{i\,HF}^N$ describes the Hartree-Fock-energy, cf. Chapter 5 of the lectures in Molecular Physics. The Hartree-Fock-approximation is based on the Slater determinant for wave functions of the electrons which are assumed to be independent from each other. The value of correlation energy, which has been neglected in the HF description of the interaction amongst the electrons, is given as $E_{i\,correlation}^N$.

In a similar method we can also describe the ionized state $E_f^{N-1}(k)$. But it has to be taken into account that there is an electron missing in the *k*-state, and that the electrons have already reoriented and rearranged themselves after a vacancy was created. If we describe $E_f^{N-1}(k)$ by the Hartree-Fock approximation, $E_{f\,HF}^{N-1}(k)$, with the same electron function (other than the *k*-function) as for the $E_{i\,HF}^N$ (frozen orbital approximation), then we have to correct the value of the obtained energy by a value $E_{relaxation}(k)$ which is denoted as the relaxation energy:

$$E_{f\,HF}^{N-1}(k) = E_{f\,HF}^{N-1}(k)^{frozen} + E_{relaxation}(k). \tag{8.12}$$

Taking into account the relativistic effects we obtain the following relation for the binding energies of the vertical transitions $E_B(k)$:

$$E_B(k) = E_f^{N-1}(k) - E_i^N = -\varepsilon(k) + E_{relaxation}(k) + \Delta E_{correlation}(k) + \Delta E_{relativistic}(k). \tag{8.13}$$

The terms $\Delta E_{correlation}$ and $\Delta E_{relativistic}$ stands for the changes between the initial and the final states in the correlation energy and the relativistic effects, respectively. The last three contributions am,ounts around 10% of the total binding energy.

As an example, we consider the 1s-electron of neon:
$-\varepsilon$ = 891,7 eV; $E_{relaxation}$ = 23,1 eV; $\Delta E_{correlation}$ = 0,6 eV; $\Delta E_{relativistic}$ = 0,8 eV; I_{1s} = 870 eV.

In general we have

- for **inner shells:** $E_{relaxation} > 10\ \Delta E_{correlation}$,
- and for **valence shells:** $E_{relaxation} \approx \Delta E_{correlation}$.

Chemical bonds much stronger influence the valence electrons than inner electrons. Inspite of that, the chemical shift of the binding energy $\Delta E_B(k)$ of inner electrons is investigated by ESCA. Now we consider the influence of two different bonding types a and b on the ionization energies of an orbital *k*:

$$\Delta E_B(k) = E_B^a(k) - E_B^b(k) = -\Delta\varepsilon(k) + \Delta E_{relaxation}(k) + \Delta^2 E_{correlation}(k) + \Delta^2 E_{relativistic}(k). \tag{8.14}$$

$\Delta E_B(k)$ lies in the range of few eV. A pure charge consideration gives us for the relation of the binding energy of the *k*-orbital of an atom indexed by *i*:

$$E_i = E_i^0 + \alpha q_i + eV_i \quad \text{with} \quad V_i = \sum_{j \neq i} \frac{q_j}{r_{ji}}. \tag{8.15}$$

E_i^0 is the reference energy, α a factor und q_i the charge at position of the atom *i* at the position of the atom *j*. The value r_{ji} denotes the distances between the atoms. Comparing compouhnds having small differences in their binding energies we obtain

$$\Delta E_B(k) = -\Delta\varepsilon(k) \propto \Delta V. \tag{8.16}$$

This chemical shift depends on the difference in charges at the position of the neighboring nuclei and through that a good co-relation between electro-negativity of the bonding results.

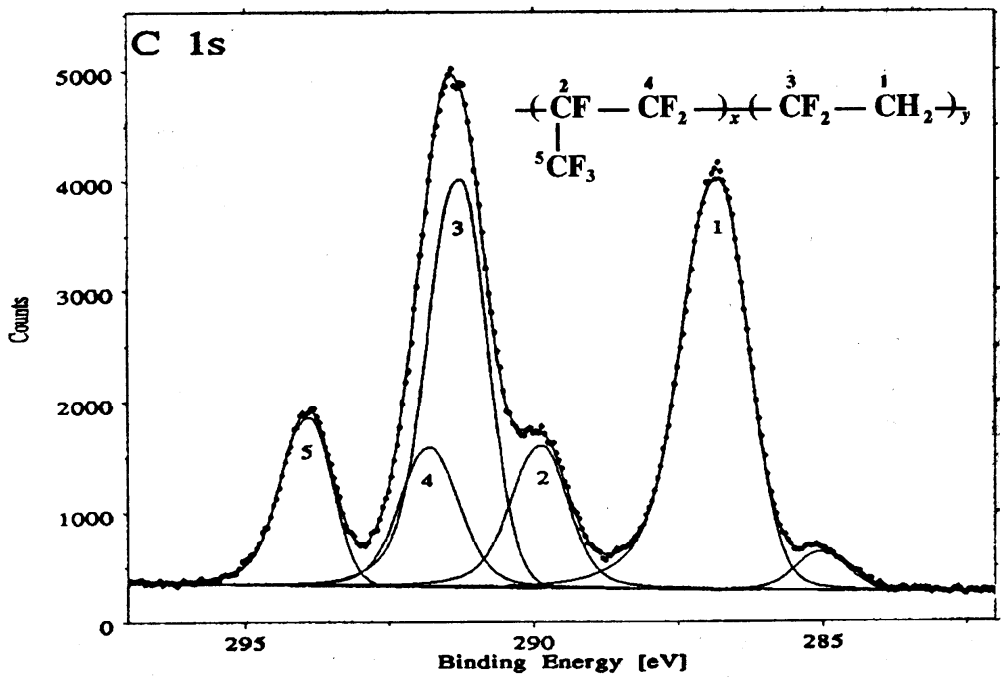

F

ig. 8.17 XPS-Spektrum of a C 1s-electron of the co-polymer Viton A^{TM} (DuPont). The peak at 285 eV gives an idea about the contamination due to carbon monoxide. Taken from David Briggs, S. 45, see Literature.

8.4 Auger electron spectroscopy, AES

The Auger effect, named after the French physicist Pierre Auger, is a two-step process, in a manner similar to the techniques of X-ray fluorescence spectroscopy. (Single-step processes in contrast are X-ray emission and photoelectron spectroscopy.) First, a hole is created due to escape of an electron from any of the inner electron shells, e. g. K-shell, due to bombardment by an electron beam. Second, an electron from a shell above, e. g. L-shell, falls non-radiating into the hole that was created in inner shell in first step. Part of the energy that is liberated by this transition from L to K is enough to cause the excitation of another electron from the L-shell which allows it to escape as a photoelectron.

As a result of the above two process in succession a doubly charged particle or atom is left behind. The Auger effects is also referred to, or called as, an inner photoelectron effect.

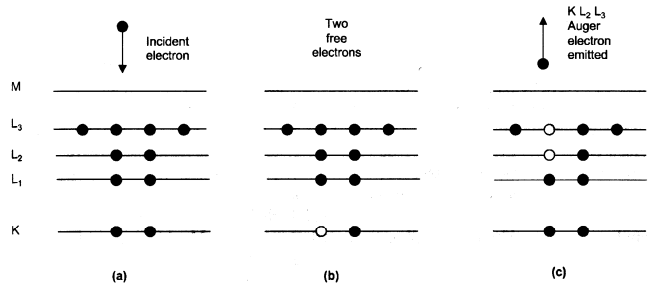

Fig. 8.18 Schematic of a KL_2L_3-Auger process, taken from J.T. Grant, see Literature.

An example for labeling of the Auger electron is Mg-KL_2L_3, where the first letter denotes the element, the second letter the primary hole, the fourth letter the auger electron created.
In case that both the electrons (here L_2L_3) are in valence bands the notation used is KVV. The letter frequently used to denote the inner core-level electrons is C, so that the notation for auger-electron becomes CV'. Derivative spectra are usually recorded and analyzed. For this the phase sensitive lock-in-amplifier operates in the low-frequency ranges of some kHz. The energy analyzer voltage is modulated with the same frequency. This procedure removes the base line shift of the photoelectron spectrum which is caused by the inelastic scattering of the electrons.

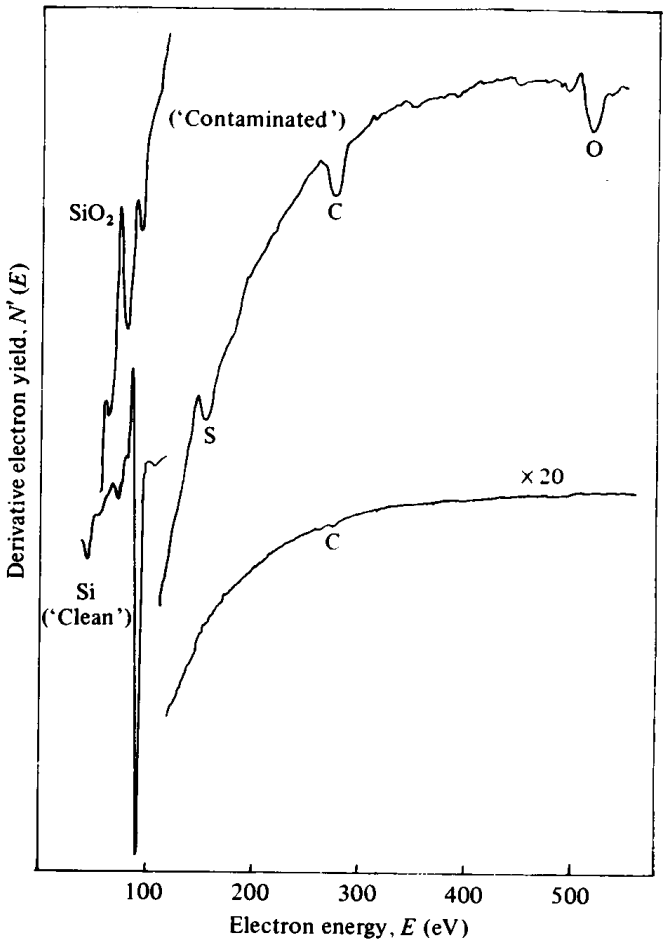

Fig. 8.19 Derivative Auger spectra from clean and contaminated Si samples. Auger peaks for the impurity species are labeled. Note the difference in the Si L2,3VV Auger transitions. The contaminated surface shows this peak dominated by the line shape characteristics of SiO_2. Taken from Woodruff and Delchar Fig. 3.34, see Literature.

The costs of instruments used in Auger spectroscopy techniques amount to a few hundred thousand Dollars. The equipment for AES are either constructed as a stand alone version, or otherwise, as also built in combination with the instrumentation needed for XPS spectrometry (see Fig. 8.12). The energy dependence of the Auger-electrons on the energies of electrons in the sub-shells of the atoms complicates the spectrum in sharp contrast to ESCA, and this makes it relatively less suitable for the purpose of analytical investigations of electron structure in solid or condensed matter states. But advantages lie in its higher detection sensitivity for probing surface layer impurities (about 0.001 monolayers) and a higher lateral resolution between 0.1–100 µm.

8.5 Literature

Ade, H. and S. Urquhart: NEXAFS spectroscopy and microscopy of natural and synthetic polymers, in T.-SK. Sham (Editor): Chemical applications of synchrotron radiation, Part 1. World Scientific, New Jersey, 2002, S. 285-355. ISBN 981-02-4977-2

Barry, A.: in Handbook of X-Ray and Ultraviolet Photoelectron Spectroscopy ed. by D. Briggs, Hayden London 1977

Briggs, D., J.T. Grant (Edts.): Surface Analysis by Auger and X-Ray Photoelectron Spectroscopy, IM Publications and Surface Spectra Limited, Chichester and Manchester, 2003, 899 p., ISBN 1-901019-04-7

Drummond, I.W.: XPS: Instrumentation and Performance in Briggs, D., J.T. Grant (Edts.): Surface Analysis by Auger and X-Ray Photoelectron Spectroscopy, IM Publications and Surface Spectra Limited, Chichester and Manchester, 2003, p. 117-189, ISBN 1-901019-04-7

Grant, J.T.: AES, Basic Principles, Spectral Features and Qualitative Analysis, in Briggs, D., J.T. Grant (Edts.): Surface Analysis by Auger and X-Ray Photoelectron Spectroscopy, IM Publications and Surface Spectra Limited, Chichester and Manchester, 2003, 899 p., ISBN 1-901019-04-7

Heald, S.M.and D.T. Jiang: X-ray reflectivity and XAFS of thin films, in T.-SK. Sham (Editor): Chemical applications of synchrotron radiation, Part 2. World Scientific, New Jersey, 2002, S. 761-798. ISBN 981-02-4978-0

Hüfner, Stefan: Photoelectron Spectroscopy, 3rd ed., Springer, Berlin, 2003, 662 S., ISDN 3-540-41802-4

Janßen, A., J. Flock: Wellenlängendispersive Röntgenfluoreszenzspektroskopie, Chemie in Labor- und Biotechnik, 51 (2000), Heft 5

Kuzmany, Hans: Solid-State Spectroscopy, Springer, Berlin, 1998, 3-540-63913-6, Fig. 3.9

Margaritondo, G.: Introduction to Synchrotron Radiation, Oxford University Press, 1988, Fig. 2.1

Meschede, D. : Gerthsen-Physik, 22. Aufl., Springer, Berlin, Heidelberg, 2004

Rehr, J.J., A. Ankudinov, S.I. Zabinsky: High order multiple scattering theory of XAFS, in T.-SK. Sham (Editor): Chemical applications of synchrotron radiation, Part 2. World Scientific, New Jersey, 2002, S. 761-798. ISBN 981-02-4978-0

Stöhr, Joachim: NEXAFS Spectroscopy, Springer 1996 177 S. ISBN 0387544224, siehe auch http://www-ssrl.slac.stanford.edu/stohr/nexafs.htm.

Woodruff, D.P. and T.A. Delchar: Modern Techniques of Surface Science, 2nd ed., Cambridge University Press, 1994 ISBN 0 521 41467-9